IJC
International Journal of Cancer

Alterations of the spindle checkpoint pathway in clinicopathologically aggressive CpG island methylator phenotype clear cell renal cell carcinomas

Eri Arai[1], Masahiro Gotoh[1], Ying Tian[1], Hiromi Sakamoto[2], Masaya Ono[3], Akio Matsuda[4], Yoriko Takahashi[5], Sayaka Miyata[5], Hirohiko Totsuka[6], Suenori Chiku[7], Motokiyo Komiyama[8], Hiroyuki Fujimoto[8], Kenji Matsumoto[4], Tesshi Yamada[3], Teruhiko Yoshida[2] and Yae Kanai[1]

[1] Division of Molecular Pathology, National Cancer Center Research Institute, Tokyo, Japan
[2] Division of Genetics, National Cancer Center Research Institute, Tokyo, Japan
[3] Division of Chemotherapy and Clinical Research, National Cancer Center Research Institute, Tokyo, Japan
[4] Department of Allergy and Immunology, National Research Institute for Child Health and Development, Tokyo, Japan
[5] Bioscience Department, Business Development Division, Mitsui Knowledge Industry Co. Ltd., Tokyo, Japan
[6] Bioinformatics Group, Research and Development Center, Solution Division 4, Hitachi Government and Public Corporation System Engineering Ltd., Tokyo, Japan
[7] Science Solutions Division, Mizuho Information and Research Institute, Inc., Tokyo, Japan
[8] Department of Urology, National Cancer Center Hospital, Tokyo, Japan

CpG-island methylator phenotype (CIMP)-positive clear cell renal cell carcinomas (RCCs) are characterized by accumulation of DNA hypermethylation of CpG islands, clinicopathological aggressiveness and poor patient outcome. The aim of this study was to clarify the molecular pathways participating in CIMP-positive renal carcinogenesis. Genome (whole-exome and copy number), transcriptome and proteome (two-dimensional image converted analysis of liquid chromatography-mass spectrometry) analyses were performed using tissue specimens of 87 CIMP-negative and 14 CIMP-positive clear cell RCCs and corresponding specimens of non-cancerous renal cortex. Genes encoding microtubule-associated proteins, such as *DNAH2, DNAH5, DNAH10, RP1* and *HAUS8*, showed a 10% or higher incidence of genetic aberrations (non-synonymous single-nucleotide mutations and insertions/deletions) in CIMP-positive RCCs, whereas CIMP-negative RCCs lacked distinct genetic characteristics. MetaCore pathway analysis of CIMP-positive RCCs revealed that alterations of mRNA or protein expression were significantly accumulated in six pathways, all participating in the spindle checkpoint, including the "The metaphase checkpoint ($p = 1.427 \times 10^{-6}$)," "Role of Anaphase Promoting Complex in cell cycle regulation ($p = 7.444 \times 10^{-6}$)" and "Spindle assembly and chromosome separation ($p = 9.260 \times 10^{-6}$)" pathways. Quantitative RT-PCR analysis revealed that mRNA expression levels for genes included in such pathways, *i.e.*, *AURKA, AURKB, BIRC5, BUB1, CDC20, NEK2* and *SPC25*, were significantly higher in CIMP-positive than in CIMP-negative RCCs. All CIMP-positive RCCs showed overexpression of Aurora kinases, *AURKA* and *AURKB*, and this overexpression was mainly attributable to increased copy number. These data suggest that abnormalities of the spindle checkpoint pathway participate in CIMP-positive renal carcinogenesis, and that *AURKA* and *AURKB* may be potential therapeutic targets in more aggressive CIMP-positive RCCs.

Key words: aurora kinases, spindle checkpoint, clear cell renal cell carcinoma (RCC), CpG island methylator phenotype (CIMP), multi-layer omics analysis

Abbreviations: 2DICAL: two-dimensional image converted analysis of liquid chromatography-mass spectrometry; ASCAT: allele-specific copy number analysis of tumors; CIMP: CpG island methylator phenotype; GeMDBJ: the Genome Medicine Database of Japan; GPHMM: Global Parameter Hidden Markov Model; indel: insertion/deletion; N: non-cancerous renal cortex tissue; NCBI: National Center for Biotechnology Information; PolyPhen: polymorphism phenotyping; RCC: renal cell carcinoma; SIFT: sorting intolerant from tolerant; SNP: single-nucleotide polymorphism; T: tumorous tissue; TNM: tumor-node-metastasis

Additional Supporting Information may be found in the online version of this article.

Grant sponsor: Program for Promotion of Fundamental Studies in Health Sciences of the National Institute of Biomedical Innovation (NiBio); **Grant number:** 10-41, 10-42, 10-43 and 10-44; **Grant sponsor:** Grant-in-Aid for the Third Term Comprehensive 10-Year Strategy for Cancer Control from the Ministry of Health, Labor and Welfare of Japan; **Grant number:** 22090291; **Grant sponsor:** Grants-in-Aid for Scientific Research (B) and (C) from the Japan Society for the Promotion of Science (JSPS); **Grant number:** 23390096 and 25460487
DOI: 10.1002/ijc.29630
History: Received 21 Aug 2014; Accepted 20 May 2015; Online 8 June 2015
Correspondence to: Yae Kanai, Division of Molecular Pathology, National Cancer Center Research Institute, 5-1-1 Tsukiji, Chuo-ku, Tokyo 104-0045, Japan. Tel.: 81-3-3542-2511, Fax: 81-3-3248-2463, E-mail: ykanai@ncc.go.jp

What's new?

CpG-island methylator phenotype (CIMP)-positive clear cell renal cell carcinomas (RCCs) are characterized by an accumulation of DNA hypermethylation of CpG islands, clinicopathological aggressiveness, and poor patient outcome. The molecular pathways responsible for generating CIMP-positive clear cell RCCs, however, remain unclear. Based on an integrated multilayer omics approach including genome, transcriptome, and proteome analyses, here the authors show that abnormalities in the spindle checkpoint pathway participate in CIMP-positive renal carcinogenesis. The results also suggest the aurora kinases AURKA and AURKB as potential therapeutic targets in more aggressive CIMP-positive RCCs.

Not only genetic, but also epigenetic events appear to accumulate during carcinogenesis, and both types of event in association with each other reflect the clinicopathological diversity of cancers.[1,2] DNA methylation alterations are among the most consistent epigenetic changes in human cancers.[3,4] In well-studied cancers[5] such as colorectal cancer[6] and stomach cancer,[7] a distinct phenotype, which is significantly correlated with clinicopathological characteristics and involves accumulation of DNA hypermethylation of CpG islands, is defined as the CpG island methylator phenotype (CIMP).

Clear cell renal cell carcinoma (RCC) is derived from the proximal tubule, and is the most common histological subtype of kidney cancer in adults.[8] It has been shown that DNA methylation alterations play a significant role in renal carcinogenesis.[9,10] Although Morris and Maher previously reported that the relevance of the CIMP-positive phenotype to RCCs had not yet been clearly defined,[11] we first identified CIMP-positive clear cell RCCs based on genome-wide DNA methylation (methylome) analysis[12] and showed that DNA hypermethylation of CpG islands in the *FAM150A, GRM6, ZNF540, ZFP42, ZNF154, RIMS4, PCDHAC1, KHDRBS2, ASCL2, KCNQ1, PRAC, WNT3A, TRH, FAM78A, ZNF671, SLC13A5* and *NKX6-2* genes was the hallmark of CIMP in RCCs.[13]

CIMP-positive clear cell RCCs are clinicopathologically aggressive tumors: they have a larger diameter, show more frequent vascular involvement, infiltrating growth, and renal pelvis invasion, and also have higher histological grades and pathological TNM stages than CIMP-negative RCCs.[13] During the follow-up period after nephrectomy, the cancer-free and overall survival rates of patients with CIMP-positive clear cell RCCs have been shown to be significantly lower than those of patients with CIMP-negative clear cell RCCs.[13] Therefore, the molecular pathways responsible for generating CIMP-positive clear cell RCCs should be clarified, and therapeutic targets for affected patients should be identified.

Multilayer-omics analysis, involving genome, methylome, transcriptome and proteome analyses of the same tissue specimens, can be a powerful tool for revealing pathways that play a significant role in carcinogenesis.[14] In order to clarify the molecular pathways involved in CIMP-positive renal carcinogenesis and to identify therapeutic targets for CIMP-positive clear cell RCCs, we performed genome (whole-exome and copy number), transcriptome and proteome analyses in 87 CIMP-negative and 14 CIMP-positive clear cell RCCs.

Material and Methods

Tissue samples and methylome analysis

In our previous study, CIMP in the initial cohort was defined by unsupervised hierarchical clustering (Euclidean distance, Ward's method) based on single-CpG resolution methylome analysis using the Infinium HumanMethylation27 Bead Array (Illumina, San Diego, CA).[13] As the initial cohort, we used 87 paired samples of non-cancerous renal cortex tissue (N) and tumorous tissue (T) obtained from 87 patients with CIMP-negative clear cell RCCs and 14 paired samples of N and T obtained from 14 patients with CIMP-positive clear cell RCCs, giving a total of 101 paired samples of N and T. These patients did not receive preoperative treatment and underwent nephrectomy at the National Cancer Center Hospital, Tokyo, Japan. Histological diagnosis was made in accordance with the World Health Organization classification.[15] All the tumors were graded on the basis of previously described criteria[16] and classified according to the pathological Tumor-Node-Metastasis (TNM) classification.[17] Clinicopathological parameters of CIMP-negative and CIMP-positive patients are summarized in Table 1.

In our previous study, we quantitatively evaluated the DNA methylation levels of 299 CpG sites on the 17 RCC-specific CIMP marker genes and established diagnostic criteria for reproducible diagnosis of CIMP-positive RCCs using receiver operating characteristic curve analysis.[18] Using these criteria, we additionally identified five CIMP-positive RCCs from the second cohort ($n = 100$).[18] Five CIMP-positive RCCs from the second cohort were also included in this study and their clinicopathological parameters are summarized in Table 1.

All patients included in this study provided written informed consent. This study was approved by the Ethics Committee of the National Cancer Center, Tokyo, and was performed in accordance with the Declaration of Helsinki.

Exome analysis

Whole exome analysis of genomic DNA was performed for the 101 paired samples from the initial cohort and the five paired samples from the second cohort using SureSelect Human All Exon 50 Mb (Agilent Technologies, Santa Clara,

Table 1. Clinicopathological parameters of the examined CpG island methylator phenotype (CIMP)-negative and CIMP-positive clear cell renal cell carcinomas (RCCs)

Clinicopathological parameters		Initial cohort		Second cohort
		CIMP-negative RCCs (n = 87)	CIMP-positive RCCs (n = 14)	CIMP-positive RCCs (n = 5)
Age		62.20 ± 10.24	67.36 ± 11.06	62.20 ± 7.92
Sex	Male	60	11	3
	Female	27	3	2
Tumor diameter (cm)		5.21 ± 3.19	8.75 ± 2.85	8.26 ± 3.91
Predominant histological grades[1]	G1	46	1	0
	G2	33	4	1
	G3	7	7	2
	G4	1	2	2
Highest histological grades[2]	G1	7	0	0
	G2	41	1	0
	G3	24	4	1
	G4	15	9	4
Vascular involvement	Negative	51	1	0
	Positive	36	13	5
Renal vein tumor thrombi	Negative	66	5	0
	Positive	21	9	5
Predominant growth pattern[1]	Expansive	81	7	3
	Infiltrative	6	7	2
Most aggressive growth pattern[2]	Expansive	55	4	3
	Infiltrative	32	10	2
Tumor necrosis	Negative	68	2	1
	Positive	19	12	4
Invasion to renal pelvis	Negative	80	10	3
	Positive	7	4	2
Pathological TNM stage	Stage I	47	0	0
	Stage II	1	1	0
	Stage III	23	9	4
	Stage IV	16	4	1

[1]If the tumor showed heterogeneity, findings in the predominant area were described
[2]If the tumor showed heterogeneity, the most aggressive features of the tumor were described.

CA) and the Illumina HiSeq 2000 platform. Somatic non-synonymous single-nucleotide mutations and insertions/deletions (indels) were called as described previously.[19,20] Effects of amino acid substitutions on protein function due to single-nucleotide non-synonymous mutations have been estimated using the Sorting Intolerant from Tolerant (SIFT) (http://sift.jcvi.org)[21] and Polymorphism Phenotyping (PolyPhen)-2 (http://genetics.bwh.harvard.edu/pph2/),[22] and those due to indels have been estimated using SIFT.[23] All data from exome analysis will be submitted to the Genome Medicine Database of Japan (GeMDBJ, https://gemdbj.nibio.go.jp/dgdb/). Data from whole-exome analysis of 66 RCCs included in the initial cohort have been published in another article[19] not focusing on CIMP.

Sanger sequencing

To verify the non-synonymous single-nucleotide mutations and indels of genes showing an incidence of genetic aberration of 10% or more in CIMP-negative and CIMP-positive RCCs in the initial cohort by exome analysis, the target sites and the flanking sequences of each patient's DNA template were amplified individually with specific primers designed

using Primer6.0. The PCR products were then sequenced with an ABI 3730 DNA Analyzer using the BigDye Terminator v1.1 Cycle Sequencing kit (Life Technologies, Carlsbad, CA).

Single-nucleotide polymorphism (SNP) microarray analysis

SNP microarray analysis of genomic DNA was performed for the 101 paired samples from the initial cohort and the 5 paired samples from the second cohort using the HumanOmni1-Quad BeadChip system (Illumina) as described previously.[19] Copy number data had been obtained using Allele-Specific Copy Number Analysis of Tumors (ASCAT) (http://heim.ifi.uio.no/bioinf/Projects/ASCAT/)[24] and Global Parameter Hidden Markov Model (GPHMM) (http://bioinformatics.ustc.edu.cn/gphmm/)[25] software. All data from SNP microarray analysis will be submitted to GeMDBJ. Data from SNP microarray analysis of 66 RCCs included in the initial cohort have been published in another article[19] not focusing on CIMP.

Expression microarray analysis

The 95 paired samples of N and T from the initial cohort, from which total RNA samples were available, were subjected to expression microarray analysis. Total RNA was isolated using TRIzol reagent (Life Technologies). Two hundred-nanogram aliquots of total RNA were used for the production of fluorescent complementary RNA, and all samples were hybridized to the SurePrint G3 Human Gene Expression 8 × 60K microarray (Agilent Technologies). The signal values were extracted using the Feature Extraction software (Agilent Technologies). The expression level (E value) of each gene was expressed as the log2-signal intensity. If the average E_T was significantly higher than the average E_N (Welch t test, $p < 0.05$), and ΔE ($E_T - E_N$) was 2 or more, the mRNA expression of the gene was considered to be elevated in T samples relative to N samples. If the average E_T was significantly lower than the average E_N (Welch t test, $p < 0.05$), and the ΔE ($E_T - E_N$) was -2 or less, the mRNA expression of the gene was considered to be reduced in T samples relative to N samples. All data from expression microarray analysis will be submitted to GeMDBJ.

Two-dimensional image converted analysis of liquid chromatography-mass spectrometry (2DICAL)

The 42 paired samples of N and T from the initial cohort, for which protein samples were available, were subjected to 2DICAL analysis.[26] One milligram of frozen tissue was digested using trypsin with 1% sodium deoxycholate, and the digested peptides were extracted in aqueous phase according to the phase transfer surfactant protocol.[27] The extracted peptide samples were dried and dissolved in 0.1% formic acid to the final concentration of 150 ng/ml, and analyzed in duplicate by nanoflow high-performance liquid chromatography (NanoFrontier nLC, Hitachi High-technologies, Tokyo, Japan) connected to an electrospray ionization quadrupole time-of-flight mass spectrometer (TripleTof 5600, AB Sciex, Framingham, MA). Mass spectrum peaks were detected, normalized, and quantified using our 2DICAL software package.[26] If the ratio of the expression level of T to the corresponding N ($P_{T/N}$) was 2 or more, the protein expression of the gene was considered to be elevated in the T sample relative to the N sample. If the $P_{T/N}$ was 0.5 or less, the protein expression of the gene was considered to be reduced in the T sample relative to the N sample. All data from 2DICAL analysis will be submitted to GeMDBJ.

Pathway analysis

MetaCore pathway analysis (http://www.genego.com) by GeneGo was performed among genes showing elevated ($p < 0.05$ and ΔE [$E_T - E_N$] of 2 or more) or reduced ($p < 0.05$ and ΔE [$E_T - E_N$] of -2 or less) mRNA expression only in CIMP-negative RCCs or genes showing a 50% or higher incidence of elevated ($P_T/_N$ of 2 or more) or reduced ($P_T/_N$ of 0.5 or less) protein expression only in CIMP-negative RCCs. MetaCore pathway analysis was also performed among genes showing elevated or reduced mRNA expression only in CIMP-positive RCCs in the initial cohort or genes showing a 50% or more incidence of elevated or reduced protein expression only in CIMP-positive RCCs in the initial cohort.

Quantitative RT-PCR analysis

The 88 paired samples of N and T from the initial cohort, from which additional total RNA samples were available even after the expression microarray analysis, and the five paired samples of N and T from the second cohort were subjected to quantitative RT-PCR analysis. cDNA was reverse-transcribed from total RNA using random primers and Superscript III RNase H$^-$Reverse Transcriptase (Life Technologies). Levels of expression of mRNA for the *AURKA, AURKB, AURKC, BIRC5, BUB1, CDC20, NEK2* and *SPC25* genes were analyzed using custom TaqMan Expression Assays on the 7500 Fast Real-Time PCR System (Life Technologies) employing the relative standard curve method. The probes and PCR primer sets employed are summarized in Supporting Information Table S1. Experiments were performed in triplicate, and the mean value for the three experiments was used as the CT value. All CT values were normalized to that of *GAPDH* in the same sample. If the ratio of the expression level of T to that of the corresponding N ($CT_{T/N}$) was 4 or more, the mRNA expression of the gene was considered to be elevated in the T sample relative to the N sample. If the $CT_{T/N}$ was 0.25 or less, the mRNA expression of the gene was considered to be reduced in the T sample relative to the N sample.

Cell culture

The KMRC-2 renal cancer cell line was maintained in Dulbecco's Modified Eagle Medium-high glucose (Sigma-Aldrich, Ontario, Canada), and the renal cancer cell lines 769-P and 786-O were maintained in RPMI-1640 (Sigma-Aldrich), both

supplemented with 10% fetal bovine serum, under 95% air and 5% CO_2 at 37°C.

Transfection with small interfering RNA (siRNA)

Cells were seeded in a 96-well plate at a concentration of 1×10^4 cells/well. When cells had reached about 60% confluence, the medium was replaced with Opti-MEM® I Reduced Serum Medium (Life Technologies). The cells were then transfected with either the Silence Select Negative Control #1 siRNA, *AURKA* miRNA or *AURKB* miRNA (Life Technologies) using Lipofectamine™ RNAiMAX reagent (Life Technologies) in accordance with the manufacturer's protocol. At 72 h after transfection, the expression level of mRNA for *AURKA* and *AURKB* was determined by quantitative real-time RT-PCR analysis. Transfected cells were then subjected to the MTS cell viability assay, cytotoxicity assay and cell apoptosis assay.

MTS cell viability assay

Cells transfected with control, *AURKA* and *AURKB* siRNAs were treated with CellTiter 96® Aqueous One Solution Reagent (Promega, Madison, WI) in accordance with the manufacturer's protocol. After 1 h, proliferation of the cells was measured by absorbance at 490 nm using an UltraMark Microplate Imaging System (Bio Rad, Hercules, CA). Results were presented as the mean ± standard deviation of triplicate determinations.

Cytotoxicity assay

0.1% CellTox™ Green Dye (Promega) was added to the media of cells transfected with control *AURKA* and *AURKB* siRNAs, in accordance with the manufacturer's protocol. After a 72-h incubation, changes in membrane integrity resulting from cell death were monitored by measurement of fluorescence at excitation/emission wavelengths of 485 nm/535 nm using an ARVO-X3 microplate reader (Perkin Elmer, Waltham, MA). Results were presented as the mean ± standard deviation for six determinations.

Cell apoptosis assay

Cells transfected with control, *AURKA* and *AURKB* siRNAs were treated with a Caspase-Glo® 3/7 assay kit (Promega), in accordance with the manufacturer's protocol. After a 1-h incubation, the luminescent signal was measured on an ARVO-X3 microplate reader (Perkin Elmer). Results were presented as the mean ± standard deviation of triplicate determinations.

Treatment with an inhibitor

Cells were seeded in a 96-well plate at a concentration of 3×10^3 cells/well and treated with VX-680 (0–3,000 nM, a pan Aurora Kinase inhibitor).[28] After a 72-h incubation, MTS assay was performed as described above. The viability of the untreated cells (negative controls) was considered to be 100%. The results were expressed as a percentage of absorbance relative to the negative control cells by subtracting the background absorbance of the non-cell control well. Relative viability = (experimental absorbance − background absorbance)/(absorbance of untreated controls − background absorbance) × 100%. Each data point represents the mean ± standard deviation for six determinations.

Statistics

Differences in the incidences of genetic aberrations and the incidences of overexpression or reduced expression of protein levels between sample groups were examined using Fisher's exact test and two-sample test for equality of proportions, at a significance level of $p < 0.05$. Based on expression microarray analysis and quantitative RT-PCR analysis, differences in mRNA expression levels between sample groups were examined using Welch's *t* test and Mann-Whitney *U* test, with a *p* values of less than 0.05 being considered as significant. For analysis of the expression microarray data obtained using 42,405 probes, Bonferroni correction was performed. Based on MetaCore pathway analysis, alterations in mRNA and protein expression were considered to be accumulated in pathways for which the *p* value was less than 0.05 in each of the CIMP-negative and CIMP-positive RCCs.

Results

Genetic aberrations in CIMP-negative and CIMP-positive clear cell RCCs

Average coverages in the whole-exome analysis for each sample are shown in Supporting Information Table S2 and the mean of the average coverage for the samples as a whole was 124.0. Somatic non-synonymous single-nucleotide mutations and indels of 3,828 and 537 genes were detected among the 101 clear cell RCCs, respectively. In total, 3,455 genes showed genetic aberrations (non-synonymous single-nucleotide mutations and/or indels) in RCCs in the initial cohort (Supporting Information Table S2). Genetic aberrations in the second cohort are summarized in Supporting Information Table S3. In Supporting Information Table S4, genetic aberrations in the both cohorts are summarized along with the previously described incidences of such aberrations in RCCs in the COSMIC database (http://cancer.sanger.ac.uk/cancergenome/projects/cosmic/). Among these genes, 666 (marked with the superscript "c" in Supporting Information Table S4) showed novel genetic aberrations only in our cohort, and not in the COSMIC data. On the other hand, aberrations of none of the 3,662 genes listed in Supporting Information Table S4 showed a difference in incidence of 10% or more between our cohort and the COSMIC data; the genetic aberration profiles in our cohort were generally consistent with those for the COSMIC data. Supporting Information Table S5 compares in more detail the genetic aberration profiles of the well-known *VHL*[29] and *PBRM1*[30] genes in the initial cohort with those in the COSMIC data. Multiple non-synonymous single-nucleotide mutations and/or indels were again shared

Table 2. Genes showing an incidence of genetic aberration of 10% or more in CpG island methylator phenotype (CIMP)-negative clear cell renal cell carcinomas (RCCs)

		No. tumors in which genetic aberrations, non-synonymous single nucleotide mutation (SNV), or insertion/deletion (indel), were detected (%)						Analysis in CIMP-negative RCCs				
		CIMP-negative RCCs (n = 87)			CIMP-positive RCCs in the initial and second cohorts (n = 19)			Predicted protein function[1]			Copy number aberration[2] (%)	
								Median (IQR) for SNV				
Gene name	Ref seq ID	SNV	Indel	Total	SNV	Indel	Total	SIFT	PolyPhen-2	SIFT for Indels	Loss	Gain
VHL	7,428	28	11	39 (45)	3	10	13 (68)	0.02 (0.08)	0.99 (0.14)	Damaging	77	9.2
PBRM1[3]	55,193	15	12	26 (30)	2	7	9 (47)	0.01 (0.14)	0.72 (0.60)	Damaging	75.9	6.9
TTN[3]	7,273	10	2	11 (13)	2	1	3 (16)	NA	NA	Neutral	0	28.7
KDM5C	8,242	5	4	9 (10)	1	2	3 (16)	0.07 (0.36)	0.73 (0.26)	Damaging	50.6	27.6

[1]Median and interquartile range (IQR) for SIFT score and PolyPhen-2 scores among all detected mutations of each gene (A SIFT score of <0.05 means "damaging" [Ref. 21]. PolyPhen-2 scores of >0.85 and 0.15 to 0.85 mean "probably damaging" and "possibly damaging," respectively [Ref. 22]).
[2]The incidence of loss (copy number of 1 or less) or gain (copy number of 3 or more) detected using ASCAT or GPHMM in CIMP-negative RCCs.
[3]SNV and indel were simultaneously detected in some cases.
Abbreviations: NA: not available using SIFT or PolyPhen-2.

between our cohort and the COSMIC data, thus confirming the reliability of our whole-exome analysis.

The total number of genes showing genetic aberrations (non-synonymous single-nucleotide mutations and/or indels) in CIMP-negative ($n = 87$) and CIMP-positive RCCs ($n = 19$ in both cohorts) was 2,894 and 1,037, respectively. The average number of genes showing genetic aberrations per case in CIMP-positive RCCs (59.53 ± 43.49) was significantly higher than that in CIMP-negative RCCs (40.38 ± 16.13, $p = 1.57 \times 10^{-3}$, Student's t-test): 46 genes showed significant differences in the incidence of genetic aberrations between CIMP-negative and CIMP-positive RCCs ($p < 0.05$, marked by superscript "a" in Supporting Information Table S4), and 3,393 genes showed genetic aberrations only in CIMP-negative RCCs or only in CIMP-positive RCCs (marked by superscript "b" in Supporting Information Table S4). Seventy-six genes showed a genetic aberration incidence of 10% or more in CIMP-positive RCCs ($n = 19$), whereas only four genes did so in CIMP-negative RCCs ($n = 87$) (Tables 2 and 3). Genes encoding microtubule-associated proteins, such as *DNAH2, DNAH5, DNAH10*,[31] *RP1*[32] and *HAUS8*,[33,34] those involved in histone modification, such as *NCOA1*,[35] those involved in cell adhesion, such as *CELSR1, CELSR2*,[36] *CTNND1*,[37] *LAMC2*[38] and *TJP1*,[39] and tumor-related genes such as *BAP1*[40] and *ATM*,[41] were frequently mutated in CIMP-positive RCCs (Table 3). As shown in Tables 2 and 3, 235 genetic aberrations (173 non-synonymous single-nucleotide mutations and 62 indels) revealed by whole-exome analysis in the initial cohort were all successfully verified by Sanger sequencing. Representative electrophoretograms for Sanger sequencing are shown as Supporting Information Figure S1. Effects of amino acid substitutions due to genetic aberrations on protein function estimated using SIFT and PolyPhen-2 software are shown in Tables 2 and 3. The incidence of copy number loss (1 or less) and gain (3 or more) of the listed genes, detected using ASCAT and GPHMM software, is indicated in Tables 2 and 3.

Alterations of mRNA expression in CIMP-negative and CIMP-positive clear cell RCCs

Supporting Information Table S6 summarizes 1,920 genes that showed elevated ($p < 0.05$ and ΔE [$E_T - E_N$] of 2 or more) or reduced ($p < 0.05$ and ΔE [$E_T - E_N$] of -2 or less) levels of mRNA expression among the 95 clear cell RCCs examined (regardless of CIMP) along with the previously described levels of mRNA expression in RCCs in the GEO database (http://www.ncbi.nlm.nih.gov/geo/query/acc.cgi?acc=GSE6344). For 847 out of 1,244 genes for which data were available in the GEO database, significantly elevated or reduced expression in T samples of our cohort was validated in the GEO data (Supporting Information Table S6), indicating that the mRNA expression profiles in the T samples in our cohort were generally consistent with those in the GEO database.

Supporting Information Table S7(a) summarizes details of 297 and 215 genes that showed elevated ($p < 0.05$ and ΔE [$E_T - E_N$] of 2 or more) and reduced ($p < 0.05$ and ΔE [$E_T - E_N$] of -2 or less) levels of mRNA expression only in CIMP-negative RCCs ($n = 81$), respectively, whereas

Table 3. Genes showing an incidence of genetic aberration of 10% or more in CpG island methylator phenotype (CIMP)-positive clear cell renal cell carcinomas (RCCs)

		No. tumor in which genetic aberrations, SNV or indel, were detected (%)						Analysis in CIMP-positive RCCs				
		CIMP-negative RCCs (n = 87)			CIMP-positive RCCs in the initial and second cohorts (n = 19)			Predicted protein function[1]			Copy number aberration[2] (%)	
								Median (IQR) for SNV				
Gene name	Ref seq ID	SNV	Indel	Total	SNV	Indel	Total	SIFT	PolyPhen-2	SIFT for Indels	Loss	Gain
VHL	7,428	28	11	39 (45)	3	10	13 (68)	0.00 (0.00)	1.00 (0.00)	Damaging	47.4	31.6
PBRM1[3]	55,193	15	12	26 (30)	2	7	9 (47)	0.50 (0.50)	0.87 (0.13)	Damaging	36.8	31.6
BAP1	8,314	2	1	3 (3)	3	1	4 (21)	0.00 (0.01)	1.00 (0.50)	Damaging	47.4	31.6
KDM5C	8,242	5	4	9 (10)	1	2	3 (16)	0.00 (NA)	1.00 (NA)	Damaging	26.3	31.6
BIRC6	57,448	2	1	3 (3)	3	0	3 (16)	0.04 (0.04)	NA	–	0	73.7
TTN[3]	7,273	10	2	11 (13)	2	1	3 (16)	NA	NA	Neutral	0	73.7
MTOR	2,475	5	0	5 (6)	3	0	3 (16)	0.00 (0.00)	1.00 (0.00)	–	5.3	52.6
DNAH2	14,6754	0	1	1 (1)	3	0	3 (16)	0.57 (0.43)	0.03 (0.01)	–	0	68.4
FAM111B	374,393	0	0	0 (0)	2	1	3 (16)	0.21 (0.13)	0.53 (0.23)	Damaging	0	57.9
RYR2	6,262	4	0	4 (5)	3	0	3 (16)	0.13 (0.13)	0.99 (0.01)	–	0	68.4
SETD2	29,072	2	6	8 (9)	1	1	2 (11)	NA	NA	Damaging	42.1	26.3
CUBN	8,029	4	0	4 (5)	1	1	2 (11)	0.73 (NA)	0.00 (NA)	Damaging	5.3	57.9
SPTA1	6,708	3	1	4 (5)	1	1	2 (11)	NA	NA	Damaging	0	68.4
WDFY3	23,001	2	1	3 (3)	2	0	2 (11)	0.01 (0.01)	0.98 (0.00)	–	0	36.8
NCOA1	8,648	2	0	2 (2)	2	0	2 (11)	0.00 (0.00)	0.97 (0.01)	–	0	73.7
PLCE1	51,196	2	0	2 (2)	2	0	2 (11)	0.03 (0.05)	1.00 (0.00)	–	15.8	52.6
ANKRD26	22,852	1	0	1 (1)	2	0	2 (11)	0.58 (0.18)	0.04 (0.04)	–	5.3	57.9
DNAH5	1,767	1	0	1 (1)	2	0	2 (11)	0.67 (0.29)	0.08 (0.08)	–	0	73.7
FOXN2	3,344	1	0	1 (1)	1	1	2 (11)	0.08 (NA)	0.26 (NA)	Neutral	0	73.7
LRBA	987	1	0	1 (1)	2	0	2 (11)	0.56 (0.29)	0.48 (0.46)	–	0	42.1
MIS18BP1	55,320	1	0	1 (1)	1	1	2 (11)	0.18 (NA)	0.46 (NA)	Damaging	26.3	36.8
PARP8	79,668	0	0	0 (0)	2	0	2 (11)	0.07 (0.02)	0.03 (0.03)	–	0	78.9
RP1	6,101	1	0	1 (1)	2	0	2 (11)	0.04 (0.03)	0.53 (0.32)	–	5.3	68.4
ATM	472	0	0	0 (0)	1	1	2 (11)	0.00 (NA)	1.00 (NA)	NA	10.5	47.4
B4GALNT3	283,358	0	0	0 (0)	2	0	2 (11)	0.60 (0.20)	0.00 (0.00)	–	0	84.2
TICRR	90,381	0	0	0 (0)	2	0	2 (11)	0.10 (0.55)	0.74 (0.35)	–	5.3	42.1
CABIN1	23,523	0	0	0 (0)	2	0	2 (11)	0.02 (0.02)	0.81 (0.14)	–	0	63.2
CD6	923	0	0	0 (0)	2	0	2 (11)	0.29 (0.29)	0.49 (0.49)	–	0	57.9
CELSR1	9,620	0	0	0 (0)	2	0	2 (11)	0.01 (0.01)	0.85 (0.14)	–	0	63.2
CELSR2	1,952	0	0	0 (0)	2	0	2 (11)	0.26 (0.20)	0.02 (0.02)	–	5.3	73.7
CNNM4	26,504	0	0	0 (0)	2	0	2 (11)	0.46 (0.46)	0.50 (0.50)	–	0	78.9
CTNND1	1,500	0	0	0 (0)	2	0	2 (11)	0.05 (0.05)	NA	–	0	63.2
DNAH10	196,385	0	0	0 (0)	2	0	2 (11)	0.38 (0.33)	NA	–	0	84.2
EIF4G3	8,672	0	0	0 (0)	2	0	2 (11)	0.22 (0.22)	0.45 (0.45)	–	15.8	47.4
EPHA6	285,220	0	0	0 (0)	2	0	2 (11)	0.00 (0.00)	NA	–	5.3	63.2
FAM194A	131,831	0	0	0 (0)	2	0	2 (11)	0.00 (0.00)	0.66 (0.34)	–	5.3	68.4
FHAD1	114,827	0	0	0 (0)	1	1	2 (11)	0.19 (NA)	NA	Damaging	5.3	57.9

Table 3. Genes showing an incidence of genetic aberration of 10% or more in CpG island methylator phenotype (CIMP)-positive clear cell renal cell carcinomas (RCCs) (Continued)

		No. tumor in which genetic aberrations, SNV or indel, were detected (%)						Analysis in CIMP-positive RCCs				
		CIMP-negative RCCs (n = 87)			CIMP-positive RCCs in the initial and second cohorts (n = 19)			Predicted protein function[1]			Copy number aberration[2] (%)	
								Median (IQR) for SNV				
Gene name	Ref seq ID	SNV	Indel	Total	SNV	Indel	Total	SIFT	PolyPhen-2	SIFT for Indels	Loss	Gain
HAUS8	93,323	0	0	0 (0)	2	0	2 (11)	0.01 (0.01)	0.98 (0.01)	–	0	68.4
HIP1	3,092	0	0	0 (0)	2	0	2 (11)	0.02 (0.00)	0.99 (0.00)	–	0	84.2
LAMC2	3,918	0	0	0 (0)	2	0	2 (11)	0.31 (0.31)	0.50 (0.50)	–	0	68.4
MED13L	23,389	0	0	0 (0)	2	0	2 (11)	0.02 (0.02)	0.99 (0.00)	–	0	84.2
PCDHGB3	56,102	0	0	0 (0)	2	0	2 (11)	NA	NA	–	0	89.5
POLR2A	5,430	0	0	0 (0)	2	0	2 (11)	0.39 (0.14)	0.93 (0.05)	–	0	68.4
SLC25A12	8,604	0	0	0 (0)	2	0	2 (11)	0.25 (0.25)	0.50 (0.50)	–	0	73.7
TJP1	7,082	0	0	0 (0)	2	0	2 (11)	0.04 (0.04)	0.49 (0.48)	–	10.5	52.6
TNFSF11	8,600	0	0	0 (0)	1	1	2 (11)	0.60 (NA)	0.00 (NA)	Damaging	15.8	47.4
ZZZ3	26,009	0	0	0 (0)	2	0	2 (11)	0.02 (0.01)	0.45 (0.44)	–	5.3	57.9
KIF26B	55,083	2	0	2 (2)	2	0	2 (11)	0.27 (0.27)	0.09 (NA)	–	0	68.4
CHST9	83,539	1	0	1 (1)	2	0	2 (11)	0.07 (0.06)	0.85 (0.15)	–	15.8	31.6
DIDO1	11,083	2	0	2 (2)	1	1	2 (11)	1.00 (NA)	0.00 (NA)	Damaging	0	78.9
QPCTL	54,814	0	0	0 (0)	1	1	2 (11)	0.00 (NA)	0.99 (NA)	Damaging	0	68.4
AMBRA1	55,626	0	0	0 (0)	2	0	2 (11)	0.01 (0.01)	0.87 (0.14)	–	0	63.2
C20orf26	26,074	0	0	0 (0)	2	0	2 (11)	0.28 (0.27)	0.86 (0.14)	–	10.5	63.2
DOPEY2	9,980	0	0	0 (0)	2	0	2 (11)	0.13 (NA)	1.00 (0.00)	–	5.3	57.9
KIAA1429	25,962	0	0	0 (0)	2	0	2 (11)	0.12 (0.12)	1.00 (NA)	–	0	73.7
RHEB	6,009	0	0	0 (0)	2	0	2 (11)	0.01 (0.01)	1.00 (0.00)	–	0	84.2
SORL1	6,653	0	0	0 (0)	2	0	2 (11)	0.03 (0.02)	0.97 (0.03)	–	10.5	57.9
STOX1	219,736	0	0	0 (0)	2	0	2 (11)	0.39 (0.19)	0.99 (0)	–	10.5	47.4
TIGD5	84,948	0	0	0 (0)	2	0	2 (11)	0.16 (0.13)	0.96 (0.03)	–	0	68.4
ZSCAN1	284,312	0	0	0 (0)	2	0	2 (11)	0.18 (0.06)	0.51 (0.48)	–	0	68.4
ACTL6B	51,412	0	0	0 (0)	2	0	2 (11)	0.54 (0.46)	NA	–	0	73.7
OGFR	11,054	0	0	0 (0)	2	0	2 (11)	0.48 (0.26)	0.43 (0.43)	–	0	78.9
OR5F1	338,674	0	0	0 (0)	2	0	2 (11)	0.52 (0.48)	0.01 (0.01)	–	0	63.2
MUC16	94,025	4	0	4 (5)	2	0	2 (11)	0.00 (0.00)	0.02 (0.02)	–	0	68.4
GPR98	84,059	2	0	2 (2)	1	1	2 (11)	0.18 (NA)	0.05 (NA)	Damaging	0	84.2
GREB1	9,687	2	0	2 (2)	1	1	2 (11)	0.00 (NA)	1.00 (NA)	Damaging	0	73.7
MORF4L2	9,643	1	0	1 (1)	1	1	2 (11)	0.00 (NA)	0.02 (NA)	Damaging	36.8	31.6
SI	6,476	2	0	2 (2)	0	2	2 (11)	–	–	Damaging	5.3	68.4
SZT2	23,334	1	0	1 (1)	1	1	2 (11)	0.03 (NA)	0.00 (NA)	NA	5.3	63.2
ABCA9	10,350	1	0	1 (1)	2	0	2 (11)	0.65 (0.36)	0.39 (0.2)	–	0	68.4
TET3	200,424	1	0	1 (1)	2	0	2 (11)	0.16 (0.15)	0.00 (NA)	–	0	73.7
AKNAD1	254,268	0	0	0 (0)	2	0	2 (11)	0.38 (0.38)	0.9 (0.1)	–	5.3	57.9
ECE1	1,889	0	0	0 (0)	1	1	2 (11)	0.00 (NA)	1.00 (NA)	Damaging	15.8	52.6
EGF	1,950	0	0	0 (0)	2	0	2 (11)	0.32 (NA)	0.08 (NA)	–	0	36.8

Table 3. Genes showing an incidence of genetic aberration of 10% or more in CpG island methylator phenotype (CIMP)-positive clear cell renal cell carcinomas (RCCs) (Continued)

		No. tumor in which genetic aberrations, SNV or indel, were detected (%)						Analysis in CIMP-positive RCCs				
		CIMP-negative RCCs ($n = 87$)			CIMP-positive RCCs in the initial and second cohorts ($n = 19$)			Predicted protein function[1]			Copy number aberration[2] (%)	
								Median (IQR) for SNV				
Gene name	Ref seq ID	SNV	Indel	Total	SNV	Indel	Total	SIFT	PolyPhen-2	SIFT for Indels	Loss	Gain
F8	2,157	0	0	0 (0)	2	0	2 (11)	0.11 (0.1)	0.5 (0.45)	–	31.6	36.8
KALRN	8,997	0	0	0 (0)	2	0	2 (11)	0.21 (0.21)	0.64 (0.36)	–	5.3	73.7

[1]Median and interquartile range (IQR) for SIFT score and PolyPhen-2 scores among all detected mutations of each gene (A SIFT score of <0.05 means "damaging" [Ref. 21]. PolyPhen-2 scores of >0.85 and 0.15 to 0.85 mean "probably damaging" and "possibly damaging," respectively [Ref. 22]).
[2]The incidence of loss (copy number of 1 or less) or gain (copy number of 3 or more) detected using ASCAT or GPHMM in CIMP positive RCCs.
[3]SNV and indel were simultaneously detected in some cases.
Abbreviations: NA: not available using SIFT or PolyPhen-2; -: SNVs or indels of the gene were not detected.

Supporting Information Table S7(b) summarizes details of 288 and 400 genes that showed elevated and reduced levels of mRNA expression only in CIMP-positive RCCs ($n = 14$), respectively. As shown in Supporting Information Table S7, 697 genes showed statistically significant differences in ΔE values between CIMP-negative and CIMP-positive RCCs ($p < 0.05$, underlined).

Alterations of protein expression in CIMP-negative and CIMP-positive clear cell RCCs

Supporting Information Table S8 summarizes 200 genes that showed elevation (average $P_{T/N}$ of 2 or more) and reduction (average $P_{T/N}$ of 0.5 or less) of protein expression among all the clear cell RCCs examined ($n = 42$, regardless of CIMP), along with the previously described Protein Atlas data (http://www.proteinatlas.org/cancer). Possibly due to differences in the analytical procedures employed, the protein expression profiles in our cohort were not completely consistent with those in the Protein Atlas database.

Supporting Information Table S9(a) summarizes details of 11 and 69 genes that showed elevation ($P_T/_N$ of 2 or more) and reduction ($P_T/_N$ of 0.5 or less) of protein expression at an incidence of 50% or more only in CIMP-negative RCCs ($n = 36$), respectively, whereas Supporting Information Table S9(b) summarizes details of 109 and 76 genes that showed elevation and reduction of protein expression at an incidence of 50% or more only in CIMP-positive RCCs ($n = 6$), respectively. As shown in Supporting Information Table S9, 95 genes showed statistically significant differences in the incidence of elevated or reduced protein expression between CIMP-negative and CIMP-positive RCCs ($p < 0.05$, underlined).

With regard to the representative proteins ANXA2 and MSH2 included in Supporting Information Table S9(b), which showed elevated and reduced protein expression, respectively, in T samples compared to N samples by 2DICAL analysis, immunohistochemical examinations were performed on tissue specimens (Supporting Information Methods). Representative photos of the immunohistochemistry are shown in Supporting Information Figure S2: elevated protein expression of ANXA2 and reduced protein expression of MSH2 in T samples relative to N samples were immunohistochemically verified, thus indicating the reliability of our 2DICAL analysis.

Pathway analysis

MetaCore pathway analysis using GeneGo was performed for 589 genes showing significantly elevated ($p < 0.05$ and ΔE $[E_T - E_N]$ of 2 or more, 297 genes in Supporting Information Table S7[a]) and significantly reduced ($p < 0.05$ and ΔE $[E_T - E_N]$ of -2 or less, 215 genes in Supporting Information Table S7[a]) mRNA expression only in CIMP-negative RCCs, and elevation ($P_T/_N$ of 2 or more, 11 genes in Supporting Information Table S9[a]) or reduction ($P_T/_N$ of 0.5 or less, 69 genes in Supporting Information Table S9[a]) of protein expression at an incidence of 50% or more only in CIMP-negative RCCs. Alterations of mRNA and protein expression were significantly accumulated in 18 GeneGo pathways ($p < 0.05$) in CIMP-negative RCCs (Table 4).

MetaCore pathway analysis using GeneGo was also performed for 865 genes showing significantly elevated ($p < 0.05$ and ΔE $[E_T - E_N]$ of 2 or more, 288 genes in Supporting Information Table S7[b]) and significantly reduced ($p < 0.05$ and ΔE $[E_T - E_N]$ of -2 or less, 400 genes in Supporting Information Table S7[b]) expression of mRNA only in CIMP-positive RCCs in the initial cohort, and elevation ($P_T/_N$ of 2 or more, 109 genes in Supporting Information Table S9[b]) and reduction ($P_T/_N$ of 0.5 or less, 76 genes in Supporting Information Table S9[b]) of protein expression at

Table 4. Statistically significant GeneGo pathway maps revealed by MetaCore pathway analysis in CpG island methylator phenotype (CIMP)-negative clear cell renal cell carcinomas (RCCs)

Pathway	*p*
Development_Transcription regulation of granulocyte development	8.627×10^{-6}
Pyruvate metabolism	2.974×10^{-4}
Glycolysis and gluconeogenesis (short map)	2.974×10^{-4}
Development_Gastrin in differentiation of the gastric mucosa	8.375×10^{-4}
Triacylglycerol metabolism p.1	3.003×10^{-3}
(L)-Arginine metabolism	5.905×10^{-3}
Transcription_Transcription regulation of aminoacid metabolism	6.635×10^{-3}
Fructose metabolism	7.818×10^{-3}
Cell adhesion_ECM remodeling	8.740×10^{-3}
Cell adhesion_Gap junctions	1.122×10^{-2}
Beta-alanine metabolism	1.206×10^{-2}
HBV signaling *via* protein kinases leading to HCC	1.346×10^{-2}
Glycolysis and gluconeogenesis p. 2	1.493×10^{-2}
Development_BMP7 in brown adipocyte differentiation	1.569×10^{-2}
G-protein signaling_RAC1 in cellular process	1.709×10^{-2}
Glycolysis and gluconeogenesis p. 1	2.144×10^{-2}
Immune response_MIF – the neuroendocrine-macrophage connector	2.144×10^{-2}
Gamma-aminobutyrate (GABA) biosynthesis and metabolism	2.794×10^{-2}

an incidence of 50% or more only in CIMP-positive RCCs in the initial cohort. Alterations of mRNA and protein expression were significantly accumulated in 47 GeneGo pathways ($p < 0.05$) in CIMP-positive RCCs (Table 5). Six pathways shown in Table 5, including the top four pathways in CIMP-positive RCCs, were all involved in the spindle checkpoint for cell cycle regulation: "Cell cycle_The metaphase checkpoint ($p = 1.427 \times 10^{-6}$)," "Cell cycle_Role of Anaphase Promoting Complex in cell cycle regulation ($p = 7.444 \times 10^{-6}$)," "Cell cycle_Spindle assembly and chromosome separation ($p = 9.260 \times 10^{-6}$)," "Cell cycle_Initiation of mitosis ($p = 1.940 \times 10^{-5}$)," "Cell cycle_Role of Nek in cell cycle regulation ($p = 8.299 \times 10^{-4}$)" and "Cell cycle_Role of Skp, Cullin, F-box containing complex in cell cycle regulation ($p = 3.003 \times 10^{-2}$)."

MetaCore pathway analysis was also performed using 434 genes included in Supporting Information Table S7(b) for which the levels of mRNA expression differed significantly between CIMP-negative and CIMP-positive RCCs (underlined in Supporting Information Table S7[b]), and 74 genes included in Supporting Information Table S9(b) for which the incidence of protein over- or under-expression differed significantly between CIMP-negative and CIMP-positive RCCs (underlined in Supporting Information Table S9[b]). The aberrations of these 508 genes showing statistically significant differences between CIMP-negative and CIMP-positive RCCs were again significantly accumulated in the above six signaling pathways, all participating in the spindle checkpoint (Supporting Information Table S10).

Table 6 lists the genes that showed overexpression at the mRNA or protein level and were involved in the above six pathways participating in the spindle checkpoint. These affected genes in the top pathway, "Cell cycle_The metaphase checkpoint ($p = 1.427 \times 10^{-6}$)," are also shown schematically in Figure 1.

Quantitative RT-PCR analysis

Levels of mRNA expression for eight genes included in the top pathway, "Cell cycle_The metaphase checkpoint ($p = 1.427 \times 10^{-6}$, Table 5 and Fig. 1)", *i.e., AURKA (Aurora-A)*,[42] *AURKB (Aurora-B)*,[43] *AURKC (Aurora-C)*,[44] *BIRC5*,[45] *BUB1*,[46] *CDC20*,[47] *NEK2*[48] and *SPC25*,[48] were quantitatively evaluated by RT-PCR analysis and added to Table 6. Levels of mRNA expression for the *AURKA*, *AURKB*, *BIRC5*, *BUB1*, *CDC20*, *NEK2* and *SPC25* genes in CIMP-positive RCCs in the initial cohort ($n = 14$) were significantly higher than in CIMP-negative RCCs ($n = 74$) ($p = 2.447 \times 10^{-4}$, 7.803×10^{-4}, 6.077×10^{-4}, 5.250×10^{-5}, 1.706×10^{-4}, 2.922×10^{-4} and 2.152×10^{-2}, respectively, Mann-Whitney *U* test, Fig. 2a). Quantitative RT-PCR analyses again revealed overexpression of mRNA for the *AURKA, AURKB, BIRC5, BUB1, CDC20, NEK2* and *SPC25* genes in the 5 CIMP-positive RCCs in the second cohort (Supporting Information Table S11). CIMP-positive RCCs from the initial and second cohorts again showed significantly higher levels of mRNA expression for the *AURKA, AURKB, BIRC5, BUB1, CDC20, NEK2* and *SPC25* genes relative to CIMP-negative RCCs (Supporting Information Fig. S3).

Knockdown experiments

Based on the DNA methylation levels of RCC-specific CIMP marker genes and the levels of mRNA expression for *AURKA* and *AURKB*, the RCC cell line KMRC-2 was considered to be a CIMP-negative model, whereas 769-P and 786-O were CIMP-positive model RCC cell lines. mRNA levels of *AURKA* and *AURKB* were successfully reduced after transfection with siRNA (Fig. 2*b*). Knockdown of *AURKA* and *AURKB* in CIMP-positive 769-P and 786-O resulted in a reduction of cell viability revealed by MTS assay, whereas no such reduction of viability was observed in CIMP-negative KMRC-2 (Fig. 2*b*). Moreover, a cytotoxicity assay revealed an increase of cell death, and an apoptosis assay revealed activation of caspase-3 and caspase-7 after knockdown of *AURKB* in 786-O (Fig. 2*b*).

Table 5. Statistically significant GeneGo pathway maps revealed by MetaCore pathway analysis in CpG island methylator phenotype (CIMP)-positive clear cell renal cell carcinomas (RCCs)

Pathway	*p*
Cell cycle_The metaphase checkpoint[1]	1.427×10^{-6}
Cell cycle_Role of Anaphase-Promoting Complex in cell cycle regulation[1]	7.444×10^{-6}
Cell cycle_Spindle assembly and chromosome separation[1]	9.260×10^{-6}
Cell cycle_Initiation of mitosis[1]	1.940×10^{-5}
Development_Regulation of cytoskeleton proteins in oligodendrocyte differentiation and myelination	5.005×10^{-5}
Cytoskeleton remodeling_Keratin filaments	5.199×10^{-5}
Development_Slit-Robo signaling	3.601×10^{-4}
Cytoskeleton remodeling_Reverse signaling by ephrin B	4.098×10^{-4}
LRRK2 in neurons in Parkinson's disease	5.236×10^{-4}
Cell cycle_Role of Nek in cell cycle regulation[1]	8.299×10^{-4}
Transport_HDL-mediated reverse cholesterol transport	1.577×10^{-3}
Cell adhesion_Histamine H1 receptor signaling in the interruption of cell barrier integrity	1.715×10^{-3}
Cell cycle_Role of 14-3-3 proteins in cell cycle regulation	1.943×10^{-3}
Reproduction_Progesterone-mediated oocyte maturation	2.328×10^{-3}
Proteolysis_Role of Parkin in the Ubiquitin-Proteasomal Pathway	2.512×10^{-3}
Chemotaxis_Inhibitory action of lipoxins on IL-8- and Leukotriene B4-induced neutrophil migration	2.729×10^{-3}
Cell adhesion_Endothelial cell contacts by junctional mechanisms	3.174×10^{-3}
Impaired inhibitory action of lipoxins on neutrophil migration in CF	3.839×10^{-3}
Cell cycle_Nucleocytoplasmic transport of CDK/Cyclins	3.872×10^{-3}
Cell adhesion_Gap junctions	4.793×10^{-3}
Regulation of CFTR activity (normal and CF)	5.533×10^{-3}
Transport_Macropinocytosis regulation by growth factors	5.857×10^{-3}
Cytoskeleton remodeling_Thyroliberin in cytoskeleton remodeling	6.283×10^{-3}
Cytoskeleton remodeling_Cytoskeleton remodeling	6.314×10^{-3}
Phenylalanine metabolism	6.542×10^{-3}
Immune response_T regulatory cell-mediated modulation of antigen-presenting cell functions	6.836×10^{-3}
Phenylalanine metabolism	7.278×10^{-3}
Cell adhesion_ECM remodeling	7.323×10^{-3}
Blood coagulation_GPCRs in platelet aggregation	8.910×10^{-3}
Apoptosis and survival_TNF-alpha-induced Caspase-8 signaling	1.308×10^{-2}
Neurophysiological process_Receptor-mediated axon growth repulsion	1.480×10^{-2}
Tyrosine metabolism p.2 (melanin)	1.518×10^{-2}
Neurophysiological process_ACM regulation of nerve impulse	1.570×10^{-2}
Cell adhesion_Chemokines and adhesion	2.797×10^{-2}
Nicotine signaling in cholinergic neurons	2.965×10^{-2}
Cell cycle_Role of Skp, Cullin, F-box containing complex in cell cycle regulation[1]	3.003×10^{-2}
Mitochondrial dysfunction in neurodegenerative diseases	3.022×10^{-2}
Oxidative stress_Role of Sirtuin1 and PGC1-alpha in activation of antioxidant defense system	3.155×10^{-2}
NF-AT signaling in cardiac hypertrophy	3.866×10^{-2}
Cytoskeleton remodeling_TGF, WNT and cytoskeletal remodeling	3.886×10^{-2}
Aberrant B-Raf signaling in melanoma progression	4.014×10^{-2}
Signal transduction_Activin A signaling regulation	4.188×10^{-2}
Immune response_IL-33 signaling pathway	4.485×10^{-2}
Development_Transcription factors in segregation of hepatocytic lineage	4.628×10^{-2}

Table 5. Statistically significant GeneGo pathway maps revealed by MetaCore pathway analysis in CpG island methylator phenotype (CIMP)-positive clear cell renal cell carcinomas (RCCs) (Continued)

Pathway	*p*
Cytoskeleton remodeling_Fibronectin-binding integrins in cell motility	4.910×10^{-2}
Histidine-glutamate-glutamine and proline metabolism	4.934×10^{-2}
Development_Regulation of endothelial progenitor cell differentiation from adult stem cells	4.986×10^{-2}

[1]Pathways involved in the spindle checkpoint for cell cycle regulation.

Treatment with an inhibitor

MTS assay revealed that treatment of CIMP-positive 769-P and 786-O cells with Aurora Kinase inhibitor VX-680 resulted in a dose-dependent reduction of cell viability, with IC_{50} values of 1.85 μM and 2.08 μM, respectively (Fig. 2*c*).

Discussion

We had previously identified CIMP-positive clear cell RCCs characterized by accumulation of DNA hypermethylation of CpG islands using methylome analysis.[13] In order to clarify molecular pathways participating in the generation of CIMP-positive clear cell RCCs and to identify therapeutic targets for patients with CIMP-positive RCCs showing a poorer outcome, multi-layer omics analysis, *i.e.,* genome, transcriptome and proteome analyses, were performed using tissue specimens of CIMP-negative and CIMP-positive RCCs and corresponding samples of non-cancerous renal cortex.

In CIMP-negative clear cell RCCs, the number of genes showing an incidence of somatic mutations of 10% or more was only four (Table 2). The incidences of somatic mutations of the four genes in CIMP-negative RCCs did not differ significantly from those of the same genes in CIMP-positive RCCs. These data indicated that CIMP-negative RCCs lacked distinct genetic characteristics.

On the other hand, CIMP-positive clear cell RCCs showed aberrations of tumor-related genes such as *BAP1*[40] and *ATM*.[41] Whether or not aberrations of genes involved in histone modification, such as *NCOA1*,[35] participate in the acquisition of epigenetic characteristics in CIMP-positive RCCs warrants further examination. Aberrations of genes involved in cell adhesion, such as *CELSR1, CELSR2*,[36] *CTNND1*,[37] *LAMC2*[38] and *TJP1*,[39] may affect the invasiveness and metastatic potential of CIMP-positive RCCs (CIMP-positive RCCs show invasive growth and distant metastasis more frequently than CIMP-negative RCCs[13]). Moreover, genetic aberrations of microtubule-associated proteins, such as *DNAH2, DNAH5, DNAH10*,[31] *RP1*[32] and *HAUS8*,[33,34] may be correlated with dysregulation of the spindle checkpoint in CIMP-positive RCCs. *DNAH2, DNAH5* and *DNAH10* encode the heavy chains of axonal dynein.[31] In mice, mutations of the axonal dynein gene *Left-right dynein (LRD)* result in abnormal segregation of sister chromatids,[49] suggesting that axonal dynein may be involved in the movement of chromosomes and positioning of the mitotic spindles for cell division. RP1 belongs to the EB1 family, which has been shown to play an important role in the regulation of microtubule dynamics and chromosome segregation.[32] *HAUS8* is phosphorylated by Aurora-A and is required for maintenance of spindle integrity and chromosomal stability in human cells.[33,34] SIFT[21,23] and PolyPhen-2[22] scores have suggested that many of the amino acid substitutions due to genetic aberrations listed in Table 3 could potentially affect protein functions in CIMP-positive RCCs.

We also performed MetaCore pathway analysis of genes showing frequent aberrations of the transcriptome (expression microarray) and/or proteome (2DICAL) to reveal the molecular pathways significantly participating in renal carcinogenesis. Even though 589 genes had shown significant alterations of mRNA and/or protein expression, MetaCore software analysis revealed that such abnormalities were accumulated in only 18 pathways in CIMP-negative RCCs (Table 4). CIMP-negative RCCs lacked not only distinct genetic characteristics but also distinct expression characteristics at both the mRNA and protein levels.

On the other hand, in CIMP-positive RCCs in the initial cohort, MetaCore pathway analysis revealed that abnormalities of the transcriptome and proteome layers were accumulated in 47 molecular pathways. Among them, six pathways including the top four were involved in the spindle checkpoint for cell cycle regulation (Table 5). Overexpression of mRNAs for the genes included in the top pathway "Cell cycle_The metaphase checkpoint ($p = 1.427 \times 10^{-6}$, Fig. 1)", *i.e., AURKA*,[42] *AURKB*,[43] *BIRC5*,[45] *BUB1*,[46] *CDC20*,[47] *NEK2*[48] and *SPC25*,[48] was confirmed using quantitative RT-PCR analysis in the same tissue specimens of CIMP-positive RCCs relative to CIMP-negative RCCs. mRNA or protein overexpression of the 27 genes involved in the above six pathways participating in the spindle checkpoint (Table 5 and Fig. 1), as well as their copy number alterations, are summarized in Table 6. All 14 CIMP-positive RCCs in the initial cohort (100%) possessed multiple abnormalities of these genes participating in the spindle checkpoint. Overexpression of mRNA for the *AURKA, AURKB, BIRC5, BUB1, CDC20, NEK2* and *SPC25* genes was confirmed even in the 5 CIMP-positive RCCs of the second cohort (Supporting Information Table S11 and Supporting Information

Table 6. Overexpression and increased copy number of genes participating in spindle checkpoint in CpG island methylator phenotype (CIMP)-positive clear cell renal cell carcinomas (RCCs)

		Case ID of CIMP-positive RCCs													
Gene symbol	Entrez Gene ID	B1	B2	B3	B4	B5	B6	B7	B8	B9	B10	B11	B12	B13	B14
AURKA	6,790	M, A (5)	M, A (7)	M, A (3)	M, A (4)	M, A (4)	M, A (4)	M	M, A (5)	M	M, A (4)	M	M, A (3)	M, A (4)	M
AURKB	9,212	M, A (3)	M, A (4)	M	M, A (4)	M, A (3)	M, A (3)	M	M, A (3)	M	M, A (3)	M	M, A (4)	M, A (3)	M
AURKC	6,795	M, A (3)	M, A (9)	M	A (4)	A (4)	M, A (3)		M, A (3)		M, A (3)	M	M, A (4)	M, A (4)	M
BIRC5	332	M, A (3)	M, A (3)	M	M, A (4)	M, A (3)	M, A (3)	M	M, A (5)	M	M, A (3)	M	M, A (4)	M, A (3)	M
BUB1	699	M, A (3)	M, A (5)	M	M, A (4)	M, A (3)	M, A (3)	M	M, A (4)	M	M, A (3)	M	M, A (4)	M, A (4)	M
CASC5	57,082	M	M, A (5)		A (3)	M	M, A (3)	M	M, A (4)	M	M	M	A (3)	A (3)	
CBX3	11,335		P		P						P				
CCNA2	890	M	M, A (6)	M	M, A (4)	M	M	M	M, A (3)	M	M	M	M, A (4)	A (3)	M
CCNB1	891	A (5)	M, A (3)	M, A (3)	M, A (4)	M, A (4)	M, A (4)	M	M, A (4)	A (3)	M, A (4)		A (5)	A (4)	
CDC20	991	M, A (3)	M, A (7)	M	M, A (4)	M, A (3)	M	M	M, A (3)	M	M, A (4)	M, L (1)	M	M, A (3)	M
CDK1	983	M, A (3)	M, A (8)	M	M, A (3)	M, A (3)	M, A (3)	M	M	M	M, A (3)	M	A (4)	A (3)	
CDT1	81,620	M, A (3)	M, A (4)	M	M, A (4)	M, A (3)	M, A (4)	M	M, A (3)	M	M	M	A (4)	A (4)	
CENPE	1,062	P, M	M	M	P, M	M	M	M	M	M	M	M	M	M	M
CENPH	64,946	M, A (5)	M, A (3)	M, A (3)	M, A (4)	M, A (4)	M, A (4)	M	M, A (4)	A (3)	M, A (4)	M	A (5)	A (4)	
HIST1H1B	3,009	P	P, A (5)	P	P, A (4)	A (3)	A (3)		A (3)		P, A (3)		A (4)	A (3)	
KIF11	3,832	M, A (3)	M, A (4)	M	A (3)	M, A (3)	M, A (3)	M, L (1)		M	M, A (3)	M	A (3)	A (3)	
KPNB1	3,837	A (3)	P, A (3)		P, A (4)	A (3)	A (3)		A (5)		P, A (3)	P	A (4)	A (3)	
LMNB1	4,001	P, M, A (4)	P, M, A (3)	P, M, A (3)	P, M, A (4)	M, A (4)	M, A (4)	M, A (3)	M, A (5)	M, A (3)	M, A (4)	P, M	A (5)	A (6)	
MAD2L1	4,085	M	M, A (6)	M	M, A (4)	M	M	M	M, A (3)	M	M	M	M, A (4)	M, A (3)	M
NDC80	10,403	M	M, A (3)	M	M, A (4)	M, A (3)	M, A (3)	M	A (4)	M	M	M		A (4)	
NEK2	4,751	M, A (3)	M, A (4)	M	M, A (4)	M, A (3)	M	M	M, A (5)	M, A (4)	M, A (4)	M	M, A (4)	M, A (4)	M
PKMYT1	9,088	M, A (3)	M, A (4)	M	M, A (4)	M, A (3)	M, A (4)	M	M, A (5)		M		A (4)	A (4)	
PLK1	5,347	A (3)	M, A (4)	M	M, A (4)	M, A (3)	A (4)	M	M, A (4)	M	M	M	A (4)	A (4)	
SPC24	147,841	M, A (3)	M, A (5)	M	M, A (4)	M, A (4)	M, A (3)		M, A (3)		A (3)		M, A (4)	A (4)	
SPC25	54,705	M, A (3)	M, A (4)	M	M, A (4)	M, A (3)	M, A (3)	M	M, A (4)	M	M, A (3)	M	M, A (4)	M, A (4)	M
TUBA1B	10,376		P		P							P			
TUBB2A	7,280		P, A (9)		P, A (4)	A (3)	A (3)		A (3)		P	P	A (4)	A (3)	

Genome and transcriptome analyses were performed in all CIMP-positive RCCs, whereas proteome analysis was performed in cases B1, B2, B3, B4, B10 and B11. M, mRNA overexpression detected by expression microarray analysis (ΔE [$E_T - E_N$] was 2 or more) and/or quantitative RT-PCR ($CT_{T/N}$ was 4 or more). P, protein overexpression detected by two-dimensional image converted analysis of liquid chromatography-mass spectrometry ($P_{T/N}$ was 2 or more). A, increased copy number detected by single nucleotide polymorphism (SNP) microarray analysis (copy number is described in parentheses). L, copy number loss detected by SNP microarray analysis (copy number is described in parentheses).

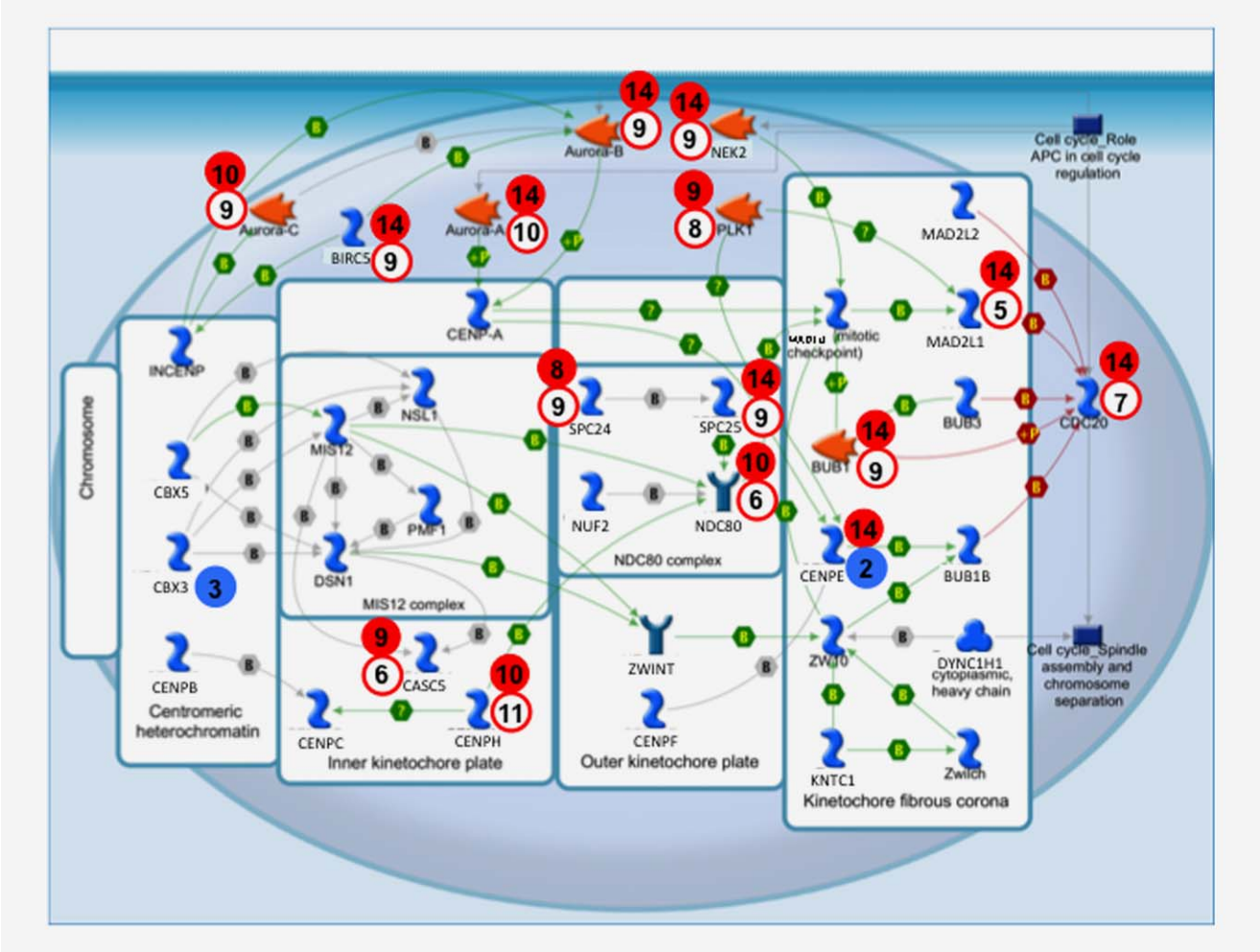

Figure 1. The top pathway "Cell cycle_The metaphase checkpoint" ($p = 1.427 \times 10^{-6}$ in Table 5) illustrated schematically using MetaCore software. mRNA overexpression (red solid circles) in tumor tissue (T) samples relative to non-cancerous renal cortex (N) samples detected by expression microarray analysis (ΔE [$E_T - E_N$] of 2 or more) and/or quantitative reverse transcription-PCR ($CT_{T/N}$ of 4 or more), protein overexpression (blue solid circles) in T samples relative to N samples detected by two-dimensional image converted analysis of liquid chromatography-mass spectrometry ($P_{T/N}$ was 2 or more) and increased copy number (red clear circles) by single nucleotide polymorphism microarray analysis of the *AURKA, AURKB, AURKC, BIRC5, BUB1, CBX3, CDC20, CASC5, CENPE, CENPH, NDC80, MAD2L1, NEK2, PLK1, SPC24* and *SPC25* genes. The number of cases with CpG island methylator phenotype (CIMP)-positive clear cell renal cell carcinomas (RCCs, $n = 14$) showing such aberrations is indicated within each circle.

Fig. S3). These data suggest that dysregulation of the spindle checkpoint plays a key role in CIMP-positive renal carcinogenesis.

It is well known that AURKA (Aurora-A) and AURKB (Aurora-B) are key kinases in the spindle checkpoint.[42,43] All 14 CIMP-positive RCCs (100%) showed overexpression of *AURKA* and *AURKB* (Table 6). ASCAT[24] and GPHMM[25] analyses based on SNP microarray data revealed that overexpression of the *AURKA* and *AURKB* genes was associated with increased copy number (3 or more) in 10 (71%) out of 14 CIMP-positive RCCs (Table 6), indicating that such overexpression was mainly attributable to increased copy number in CIMP-positive RCCs. All 5 CIMP-positive RCCs in the second cohort again showed increased copy numbers of the *AURKA* or *AURKB* genes (Supporting Information Table S11).

AURKA and AURKB could be possible therapeutic targets in CIMP-positive RCCs. Several Aurora kinase inhibitors have already been developed, and are undergoing clinical trials in patients with malignant tumors such as hematological malignancies.[50] Since CIMP-positive RCCs have a poorer outcome, CIMP diagnosis may be applicable for clinical prognostication. In addition, our CIMP diagnostic approach for clear cell RCCs may be useful as a diagnostic adjunct for personalized medicine. If CIMP diagnosis reveals CIMP negativity in tissue specimens from surgically resected materials, then the risk of recurrence and metastasis would be considered low, and the patient would not require adjuvant therapy.

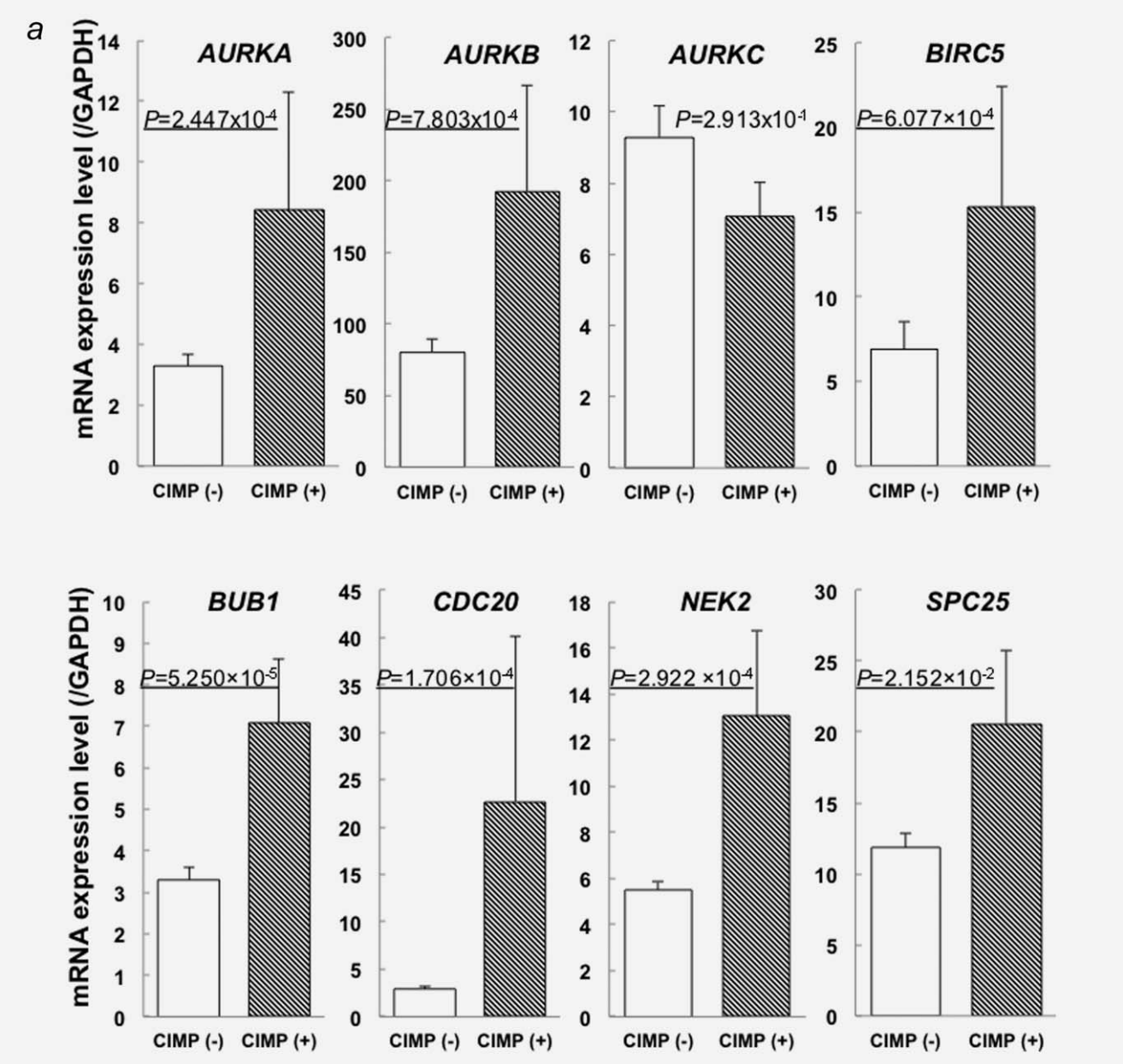

Figure 2. (*a*) Levels of mRNA expression for eight genes included in the top pathway "Cell cycle_The metaphase checkpoint" ($p = 1.427 \times 10^{-6}$ in Table 5) evaluated by quantitative reverse transcription-PCR analysis. Average levels of mRNA expression for *AURKA*, *AURKB*, *BIRC5*, *BUB1*, *CDC20*, *NEK2* and *SPC25* in CpG island methylator phenotype (CIMP)-positive renal cell carcinomas (RCCs) ($n = 14$) were significantly higher than those in CIMP-negative RCCs ($n = 74$) ($P = 2.447 \times 10^{-4}$, 7.803×10^{-4}, 6.077×10^{-4}, 5.250×10^{-5}, 1.706×10^{-4}, 2.922×10^{-4} and 2.152×10^{-2}, respectively, Mann-Whitney *U* test). −, CIMP-negative RCCs; +, CIMP-positive RCCs. Error bars, standard error. *p* values of <0.05 are underlined. (*b*) Knockdown experiments. Quantitative RT-PCR (a), MTS cell viability assay (b), cytotoxicity assay (c) and apoptosis assay (d) using renal cancer cell lines. CNTL, control siRNA; AURKA, *AURKA* siRNA; AURKB, *AURKB* siRNA. Based on the DNA methylation levels of RCC-specific CIMP marker genes and the levels of mRNA expression for *AURKA* and *AURKB*, the RCC cell line KMRC-2 was considered to be a CIMP-negative model (CIMP [−]), whereas 769-P and 786-O were CIMP-positive model (CIMP [+]) RCC cell lines. (b) Knockdown of *AURKA* and *AURKB* in 769-P and 786-O resulted in reduced cell viability, whereas such reduced viability was not observed in KMRC-2. (c) Knockdown of *AURKB* in 786-O resulted in increased cell death. (d) Knockdown of *AURKB* in 786-O resulted in increased activation of caspase-3 and caspase-7. (*c*) Treatment with the Aurora kinase inhibitor VX-680. MTS assay revealed that treatment of CIMP-positive cells with VX-680 reduced their viability, with IC_{50} values of 2.08 μM and 1.85 μM for 786-O and 769-P, respectively.

On the other hand, if surgically resected materials were shown to be CIMP-positive, the risk of recurrence and metastasis would be considered high, and Aurora kinase inhibitors might be effective in this situation. Moreover, adjuvant therapy using Aurora kinase inhibitors would be advisable immediately after nephrectomy in patients with CIMP-

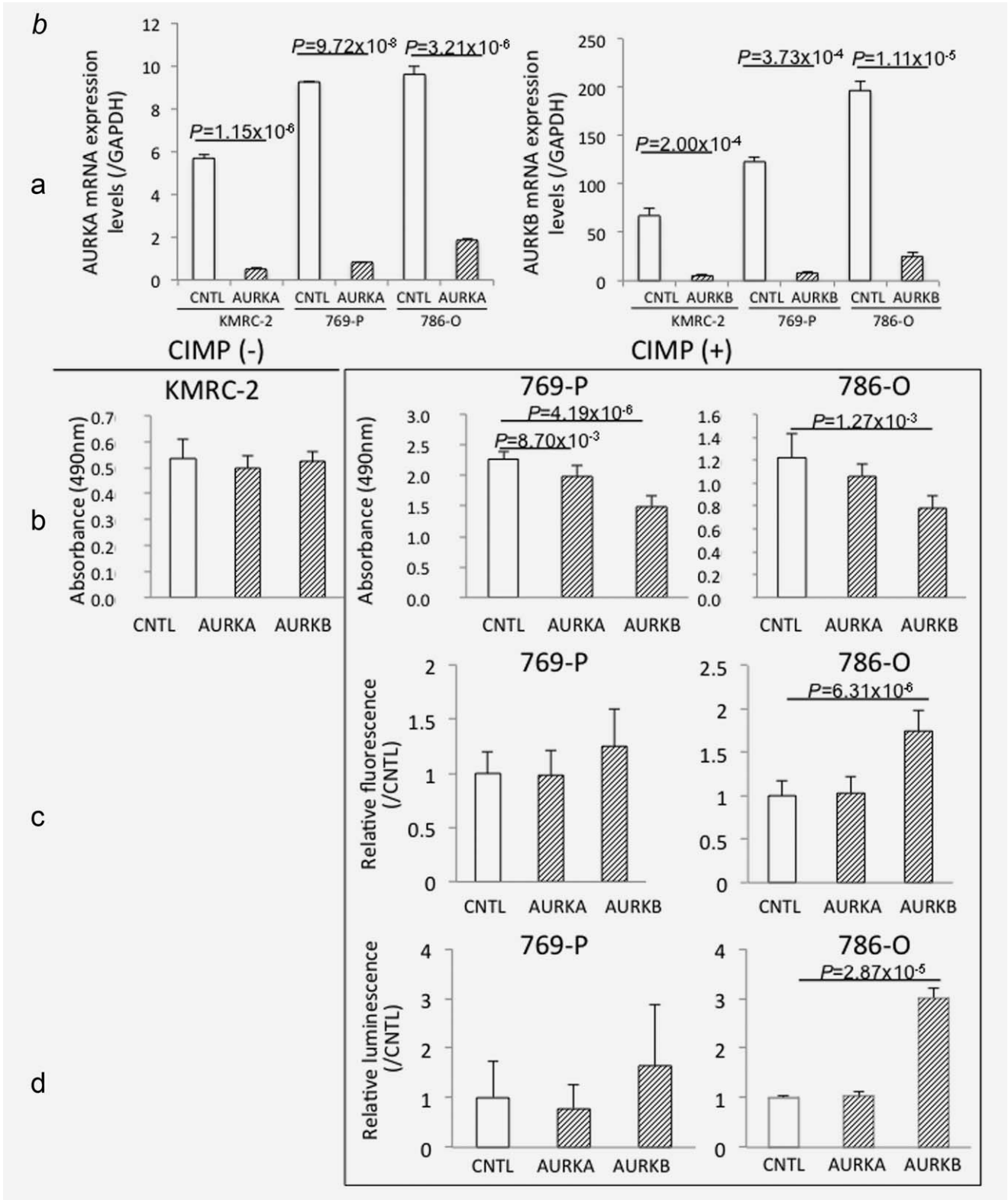

Figure 2. (Continued)

positive RCCs. Although the present data from knockdown experiments and VX-680 treatment in CIMP-positive RCC cell lines suggest the validity of adjuvant therapy for CIMP-positive RCCs using Aurora kinase inhibitors, further preclinical examinations and clinical trials will be needed before this can be considered.

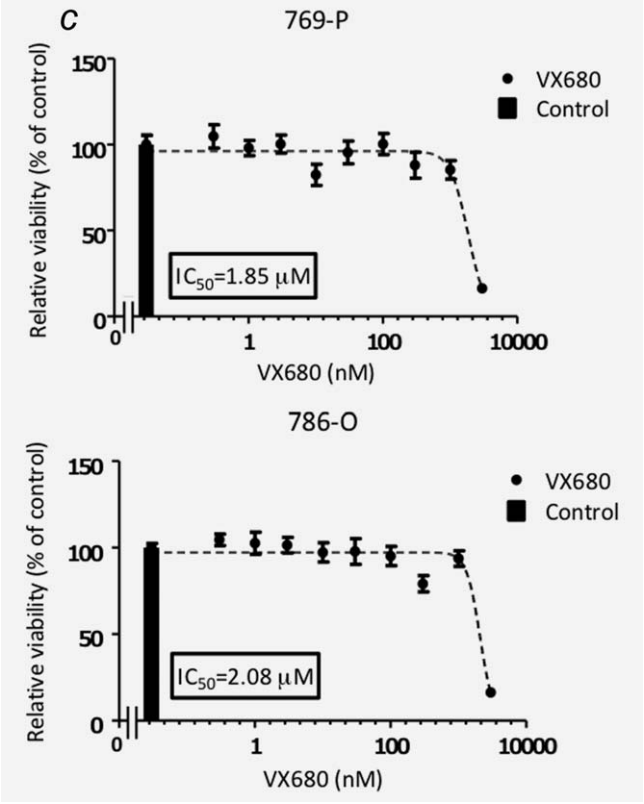

Figure 2. (Continued)

References

1. You JS, Jones PA. Cancer genetics and epigenetics: two sides of the same coin? *Cancer Cell* 2012;22:9–20.
2. Baylin SB, Jones PA. A decade of exploring the cancer epigenome - biological and translational implications. *Nat Rev Cancer* 2011;11:726–34.
3. Kanai Y. Genome-wide DNA methylation profiles in precancerous conditions and cancers. *Cancer Sci* 2010;101:36–45.
4. Arai E, Kanai Y. DNA methylation profiles in precancerous tissue and cancers: carcinogenetic risk estimation and prognostication based on DNA methylation status. *Epigenomics* 2010;2: 467–81.
5. Issa JP. CpG island methylator phenotype in cancer. *Nat Rev Cancer* 2004;4:988–93.
6. Shen L, Toyota M, Kondo Y, et al. Integrated genetic and epigenetic analysis identifies three different subclasses of colon cancer. *Proc Natl Acad Sci USA* 2007;104:18654–9.
7. Toyota M, Ahuja N, Suzuki H, et al. Aberrant methylation in gastric cancer associated with the CpG island methylator phenotype. *Cancer Res* 1999;59:5438–42.
8. Ljungberg B, Campbell SC, Choi HY, et al. The epidemiology of renal cell carcinoma. *Eur Urol* 2011;60:615–21.
9. Arai E, Kanai Y, Ushijima S, et al. Regional DNA hypermethylation and DNA methyltransferase (DNMT) 1 protein overexpression in both renal tumors and corresponding nontumorous renal tissues. *Int J Cancer* 2006;119:288–96.
10. Arai E, Ushijima S, Fujimoto H, et al. Genome-wide DNA methylation profiles in both precancerous conditions and clear cell renal cell carcinomas are correlated with malignant potential and patient outcome. *Carcinogenesis* 2009;30:214–21.
11. Morris MR, Maher ER. Epigenetics of renal cell carcinoma: the path towards new diagnostics and therapeutics. *Genome Med* 2010;2:59.
12. Bibikova M, Le J, Barnes B, et al. Genome-wide DNA methylation profiling using Infinium® assay. *Epigenomics* 2009;1:177–200.
13. Arai E, Chiku S, Mori T, et al. Single-CpG-resolution methylome analysis identifies clinicopathologically aggressive CpG island methylator phenotype clear cell renal cell carcinomas. *Carcinogenesis* 2012;33:1487–93.
14. Sato Y, Yoshizato T, Shiraishi Y, et al. Integrated molecular analysis of clear-cell renal cell carcinoma. *Nat Genet* 2013;45:860–7.
15. Eble JN, Togashi K, Pisani P. Renal cell carcinoma. In: Eble JN, Sauter G, Epstein JI, et al., eds. World Health Organization classification of tumours. Pathology and genetics. Tumours of the urinary system and male genital organs. Lyon: IARC Press, 2004. 10–43.
16. Fuhrman SA, Lasky LC, Limas C. Prognostic significance of morphologic parameters in renal cell carcinoma. *Am J Surg Pathol* 1982;6: 655–63.
17. Sobin LH, Gospodarowicz MK, Wittekind C, eds. International Union Against Cancer. TNM classification of malignant tumors, 7th ed. New York: Wiley, 2009.
18. Tian Y, Arai E, Gotoh M, et al. Prognostication of patients with clear cell renal cell carcinomas based on quantification of DNA methylation levels of CpG island methylator phenotype marker genes. *BMC Cancer* 2014;14:772.
19. Arai E, Sakamoto H, Ichikawa H, et al. Multilayer-omics analysis of renal cell carcinoma, including the whole exome, methylome and transcriptome. *Int J Cancer* 2014;135: 1330–42.
20. Wang L, Tsutsumi S, Kawaguchi T, et al. Whole-exome sequencing of human pancreatic cancers and characterization of genomic instability caused by MLH1 haploinsufficiency and complete deficiency. *Genome Res* 2012;22:208–19.
21. Ng PC, Henikoff S. Accounting for human polymorphisms predicted to affect protein function. *Genome Res* 2002;12:436–46.
22. Hicks S, Wheeler DA, Plon SE, et al. Prediction of missense mutation functionality depends on both the algorithm and sequence alignment employed. *Hum Mutat* 2011;32:661–8.
23. Sim NL, Kumar P, Hu J, et al. SIFT web server: predicting effects of amino acid substitutions on proteins. *Nucleic Acids Res* 2012;40:W452–7.
24. Van Loo P, Nordgard SH, Lingjærde OC, et al. Allele-specific copy number analysis of tumors. *Proc Natl Acad Sci USA* 2010;107:16910–15.
25. Li A, Liu Z, Lezon-Geyda K, et al. GPHMM: an integrated hidden Markov model for

identification of copy number alteration and loss of heterozygosity in complex tumor samples using whole genome SNP arrays. *Nucleic Acids Res* 2011;39:4928–41.
26. Ono M, Shitashige M, Honda K, et al. Label-free quantitative proteomics using large peptide data sets generated by nanoflow liquid chromatography and mass spectrometry. *Mol Cell Proteomics* 2006;5:1338–47.
27. Masuda T, Tomita M, Ishihama Y. Phase transfer surfactant-aided trypsin digestion for membrane proteome analysis. *J Proteome Res* 2008;7:731–40.
28. Harrington EA, Bebbington D, Moore J, et al. VX-680, a potent and selective small-molecule inhibitor of the Aurora kinases, suppresses tumor growth in vivo. *Nat Med* 2004;10:262–7.
29. Cancer Genome Atlas Research Network. Comprehensive molecular characterization of clear cell renal cell carcinoma. *Nature* 2013;499:43–9.
30. Varela I, Tarpey P, Raine K, et al. Exome sequencing identifies frequent mutation of the SWI/SNF complex gene PBRM1 in renal carcinoma. *Nature* 2011;469:539–42.
31. Chapelin C, Duriez B, Magnino F, et al. Isolation of several human axonemal dynein heavy chain genes: genomic structure of the catalytic site, phylogenetic analysis and chromosomal assignment. *FEBS Lett* 1997;412:325–30.
32. Bu W, Su LK. Regulation of microtubule assembly by human EB1 family proteins. *Oncogene* 2001;20:3185–92.
33. Tsai CY, Ngo B, Tapadia A, et al. Aurora-A phosphorylates Augmin complex component Hice1 protein at an N-terminal serine/threonine cluster to modulate its microtubule binding activity during spindle assembly. *J Biol Chem* 2011;286:30097–106.
34. Wu G, Lin YT, Wei R, et al. Hice1, a novel microtubule-associated protein required for maintenance of spindle integrity and chromosomal stability in human cells. *Mol Cell Biol* 2008;28:3652–62.
35. Dalgliesh GL Furge K, Greenman C, et al. Systematic sequencing of renal carcinoma reveals inactivation of histone modifying genes. *Nature* 2010;463:360–3.
36. Beall SA, Boekelheide K, Johnson KJ. Hybrid GPCR/cadherin (Celsr) proteins in rat testis are expressed with cell type specificity and exhibit differential Sertoli cell-germ cell adhesion activity. *J Androl* 2005;26:529–38.
37. Menke A, Giehl K. Regulation of adherens junctions by Rho GTPases and p120-catenin. *Arch Biochem Biophys* 2012;524:48–55.
38. Kwon OH, Park JL, Kim M, et al. Aberrant up-regulation of LAMB3 and LAMC2 by promoter demethylation in gastric cancer. *Biochem Biophys Res Commun* 2011;406:539–45.
39. Tsukita S, Yamazaki Y, Katsuno T, et al. Tight junction-based epithelial microenvironment and cell proliferation. *Oncogene* 2008;27:6930–8.
40. Guo G, Gui Y, Gao S, et al. Frequent mutations of genes encoding ubiquitin-mediated proteolysis pathway components in clear cell renal cell carcinoma. *Nat Genet* 2012;44:17−19.
41. Cremona CA, Behrens A. ATM signalling and cancer. *Oncogene* 2014;33:3351–60.
42. Nikonova AS Astsaturov I, Serebriiskii IG, et al. Aurora A kinase (AURKA) in normal and pathological cell division. *Cell Mol Life Sci* 2013;70:661–87.
43. Poon RY. Aurora B: hooking up with cyclin-dependent kinases. *Cell Cycle* 2013;12:1019–20.
44. Khan J, Ezan F, Crémet JY, et al. Overexpression of active Aurora-C kinase results in cell transformation and tumour formation. *PLoS One* 2011;6:e26512.
45. Li F, Ambrosini G, Chu EY, et al. Control of apoptosis and mitotic spindle checkpoint by survivin. *Nature* 1998;396:580–4.
46. Ricke RM, van Deursen JM. Aurora B hyperactivation by Bub1 overexpression promotes chromosome missegregation. *Cell Cycle* 2011;10:3645–51.
47. van Zon W, Wolthuis RM. Cyclin A and Nek2A: APC/C-Cdc20 substrates invisible to the mitotic spindle checkpoint. *Biochem Soc Trans* 2010;38:72–7.
48. Wei RR, Sorger PK Harrison SC. Molecular organization of the Ndc80 complex, an essential kinetochore component. *Proc Natl Acad Sci USA* 2005;102:5363–7.
49. Armakolas A, Klar AJ. Left-right dynein motor implicated in selective chromatid segregation in mouse cells. *Science* 2007;315:100–1.
50. Cheung CH, Coumar MS, Chang JY, et al. Aurora kinase inhibitor patents and agents in clinical testing: an update (2009-10). *Expert Opin Ther Pat* 2011;21:857–84.